Hindawi
Journal of Chemistry
Volume 2020, Article ID 1917380, 9 pages
https://doi.org/10.1155/2020/1917380

Research Article

Synthesis of Bimetallic PdAg Nanoparticles and Their Electrocatalytic Activity toward Ethanol

Fahui Gao, Yanru Yin, Zhengshuai Cao, Hongliang Li, and Peizhi Guo

Institute of Materials for Energy and Environment, State Key Laboratory of Bio-fiber and Eco-textile, College of Materials Science and Engineering, Qingdao University, Qingdao 266071, China

Correspondence should be addressed to Peizhi Guo; pzguo@qdu.edu.cn

Received 29 July 2020; Revised 2 October 2020; Accepted 25 November 2020; Published 7 December 2020

Academic Editor: Jo o Paulo Leal

Copyright © 2020 Fahui Gao et al. This is an open access article distributed under the Creative Commons Attribution License, which permits unrestricted use, distribution, and reproduction in any medium, provided the original work is properly cited.

Palladium-based bimetallic nanoparticles (NPs) have been studied as important electrocatalysts for energy conversion due to their high electrocatalytic performance and the less usage of the noble metal. Herein, well-dispersed PdAg NPs with uniform size were prepared via oil bath accompanied with the hydrothermal method. The variation of the Ag content in PdAg NPs changed the lattice constant of the face-centered cubic alloy nanostructures continuously. The Pd/Ag molar ratio in the PdAg alloy NPs affected their size and catalytic activity toward ethanol electrooxidation. Experimental data showed that PdAg NPs with less Ag content exhibited better electrocatalytic activity and durability than pure Pd NPs owing to both the small size and the synergistic effect. PdAg-acac-4 with the Pd/Ag molar ratio of 4 : 1 in the start system possessed the highest catalytic current density of 2246 mA/mg for the electrooxidation of ethanol. The differences in the morphology and electrocatalytic activity of the as-made PdAg NPs have been discussed and analyzed.

1. Introduction

Direct ethanol fuel cells (DEFCs), with many outstanding virtues, such as low toxicity, renewable capability, and low environmental pollutant emission, have been extensively studied as an ideal alternative for the energy source [1–10]. At present, the application of DEFCs in the commercial level is still limited on account of their low catalytic activity and high price of catalysts, as well as poor stability.

Platinum nanoparticles (NPs) are key electrocatalysts in commercial installations and industrial processes against conventional fossil fuels [11–13]. However, the commercialization of DEFCs based on platinum catalysts is seriously impeded by its high cost, limited natural reserves, and weak ability to resist the poisoning by the intermediate carbon monoxide (CO) produced in the ethanol oxidation reaction (EOR) [14–16]. Therefore, it is urgently needed to explore new, active, inexpensive, and stable catalysts. Nowadays, palladium (Pd) has attracted great interest as electrocatalysts owing to its good performance but relatively low cost [1–4, 6, 7, 17–26]. However, poor stability and limited active sites of Pd have seriously hindered its wider application. To improve these, structural physical features of Pd electrocatalysts including the size, shape, and composition of catalysts have been developed. A large amount of Pd nanostructured catalysts, such as cubes [27], nanoplates [28], nanowires [29], nanoflowers [30], and tetrahedra [31], have been explored and synthesized which showed high electrocatalytic activity.

Compared to single-metal nanoparticles, bimetallic alloy nanoparticles can generally exhibit better performance owing to their unique structural features, which have received extensive intension in recent years [32, 33]. Moreover, the addition of another metal reduces the loading of the palladium metal, thus decreasing the cost of the catalyst [34–38]. Various metals, such as Ni [39, 40], Fe [41, 42], Cu [43–47], Pb [48, 49], and Ag [50–52], have been used in combination with Pd to increase the electrocatalytic activity of Pd-based bimetallic or multimetallic nanocatalysts. For example, Liu et al. reported the synthesis of a Pd-Ag freestanding nanowire rich in grain boundary with both high activity and stability toward the oxygen reduction reaction (ORR) via a facile modified polyol method [51]. Peng et al. prepared a hollow raspberry-like PdAg alloy nanosphere,

which possessed high electrocatalytic activity for ethanol oxidation in alkaline media [52]. We found that ultrathin PdPb nanowires can display excellent electrocatalytic activity due to the electron transfer between Pd and Pb, lowering the d-band center and weakening the adsorption of toxic intermediates. However, the development of high-performance electrocatalysts still needs more efforts, especially for bimetallic or multimetallic nanostructures.

Herein, we report the synthesis of well-dispersed PdAg alloy nanoparticles (NPs) with uniform size via a two-step method. The formation and the composition of the PdAg alloy NPs varied with the content of silver nitrate in the start synthesis systems. The electrocatalytic performance of the catalysts related to the content of Ag in the NPs and the highest catalytic current density of the PdAg alloy can reach as high as 2246 mA/mg obtained from the start synthesis system with the molar ratio of Pd to Ag of 4 : 1. Both the particle size and the structural nature of the PdAg NPs play important roles for the electrocatalysis of ethanol.

2. Experimental Section

2.1. Materials and Reagents. All chemicals including palladium (II) acetylacetone, silver nitrate ($AgNO_3$), ethylene glycol (EG), polyvinylpyrrolidone (PVP) (molar weight = 58,000), ethanol, and acetone were analytically pure and purchased from Sinopharm Chemical Reagents. Double distilled water was used in the experiments, and ultrapure water (18.2 MΩ cm) was used throughout electrochemical measurements.

2.2. Synthesis of PdAg NP Catalysts. In a typical synthesis, 105 mg PVP was added to a bottle (30 mL) containing 8 mL double distilled water and stirred in an oil bath at 80°C for 20 minutes. Meanwhile, 61.3 mg palladium acetylacetone was stirred evenly in 3 mL double distilled water. The suspension of palladium acetylacetone and PVP solution were mixed and stirred evenly, and then, the mixture was stirred in an oil bath at 90°C for 2 hours. A certain amount of $AgNO_3$ was dissolved in 5 mL EG and mixed with the above solution; after stirred in an oil bath at 110°C for 2 hours, the mixture was transferred into a Teflon-lined stainless-steel autoclave and kept in an oven at 180°C for 10 h. After cooling down to room temperature, the products were collected by centrifugation with the addition of acetone and washed with the mixture of distilled water and ethanol several times, and then PdAg NPs were obtained after drying at 60°C for 10 h.

Four products were prepared from the start systems with the $AgNO_3$ content of 34 mg/17 mg/8.5 mg/6.8 mg, named as PdAg-acac-1/PdAg-acac-2/PdAg-acac-4/PdAg-acac-5, respectively.

2.3. Characterization. The crystallographic information and composition were investigated using a Rigaku Ultima IV X-ray diffractometer (XRD, Cu Kα radiation $\lambda = 0.15418$ nm). The morphology and structure of the samples were examined by a JEOL JSM-7800F scanning electron microscope (SEM) and a JEOL JEM-2100 Plus transmission electron microscope (TEM). High-angle annular dark-field scanning transmission electron microscopy (HAADF-STEM) coupled with energy-dispersive X-ray (EDX) elemental mappings were measured with a JEOL JEM-2100F transmission electron microscope at an accelerating voltage of 200 kV.

2.4. Electrochemical Measurements. Electrochemical measurements were conducted on a CHI660E workstation at room temperature, and the measurements of cyclic voltammetry (CV) and chronoamperometric tests were carried out with a standard three-electrode system. The details were shown in our recent reports [53].

3. Results and Discussion

Both Pd and Ag crystals have a face-centered cubic (FCC) structure. The difference in the diameters of atoms of Pd and Ag is very small; thereafter, PdAg bimetallic alloy can be easily formed and was usually reported in the literature studies recently [50]. As shown in Figure 1, the three distinct diffraction peaks of the as-made samples in the XRD patterns located between pure Pd and Ag standard patterns appeared at 38.6°, 45.3°, and 67.2°, responding to the (111), (200), and (220) crystalline planes of PdAg alloy nanoparticles, respectively. It was obvious that all the diffraction peaks of PdAg-acac-1, PdAg-acac-2, PdAg-acac-4, and PdAg-acac-5 showed a negative shift to the standard peak of pure Ag compared with that of pure Pd (JCPDS No. 46-1043), which proved the formation of the PdAg alloy [51, 52]. Moreover, the more the content of Ag, the more the negative shift of the strongest diffraction peaks at 38.6°, which indicates the addition of Ag causes the lattice expansion in the PdAg alloy compared with pure Pd. Using a Rietveld refinement, the lattice constants are about 4.02 Å, 3.99 Å, 3.95 Å, and 3.92 Å for PdAg-acac-1, PdAg-acac-2, PdAg-acac-4, and PdAg-acac-5, respectively. These indicated the gradual increase of crystal cell size with the continuous increase of the Ag content in the PdAg bimetallic nanostructures.

Figure 2 shows the SEM images of PdAg-acac-1, PdAg-acac-2, PdAg-acac-4, and PdAg-acac-5. It can be seen that each PdAg alloy is well dispersed with a narrow size distribution. All the samples are granular with the size order of PdAg-acac-1 > PdAg-acac-2 > PdAg-acac-5 > PdAg-acac-4, and the particle size of PdAg-acac-4 is significantly smaller than any of the others. The composition of elements Pd and Ag of alloy NPs was identified by SEM-EDS (Table 1), and the atomic ratios of Pd/Ag are about 0.8 : 1, 1.9 : 1, 3.4 : 1, and 4.2 : 1 for PdAg-acac-1, PdAg-acac-2, PdAg-acac-4, and PdAg-acac-5, respectively. These results are a little different from those in the start systems, more likely related to the insoluble nature of palladium acetylacetonate in ethylene glycol.

Figure 3 shows the TEM and HRTEM images of all the four PdAg NP samples. All the four types of particles have a clear boundary. Obviously, the sizes of PdAg-acac-1, PdAg-acac-2, PdAg-acac-4, and PdAg-acac-5 NPs were about

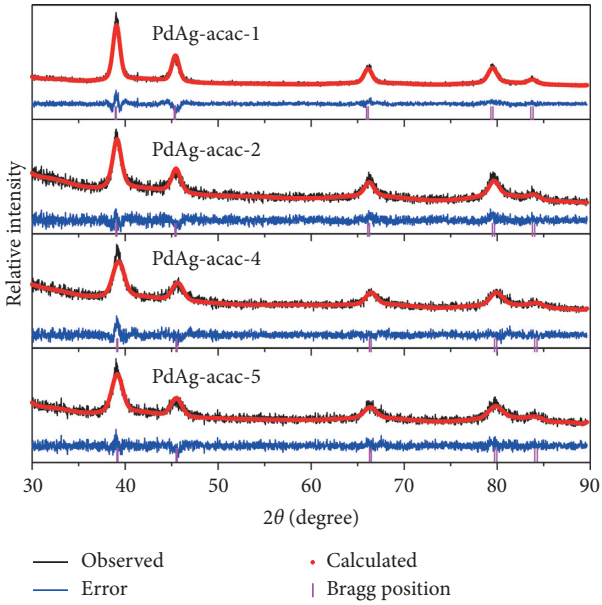

Figure 1: XRD patterns and Rietveld refinement results of PdAg-acac-1, PdAg-acac-2, PdAg-acac-4, and PdAg-acac-5.

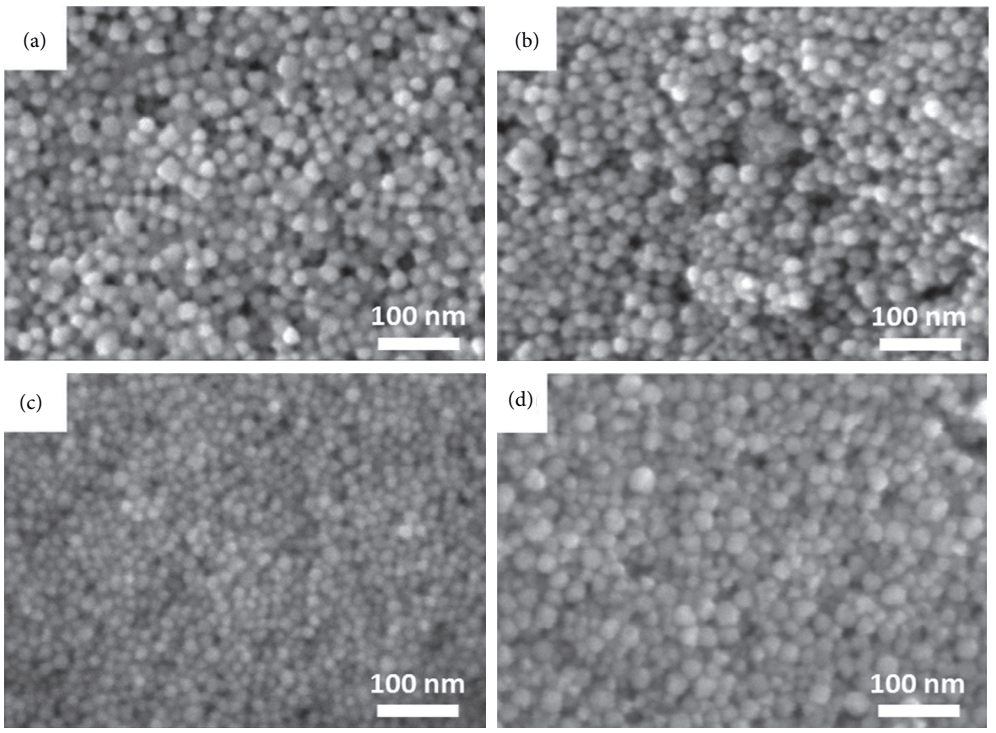

Figure 2: SEM images of PdAg-acac-1 (a), PdAg-acac-2 (b), PdAg-acac-4 (c), and PdAg-acac-5 (d).

Table 1: The atomic ratio of PdAg-acac-1, PdAg-acac-2, PdAg-acac-4, and PdAg-acac-5.

The atomic fraction	PdAg-acac-1	PdAg-acac-2	PdAg-acac-4	PdAg-acac-5
Pd (%)	44.33	65.38	76.84	80.20
Ag (%)	55.67	34.62	23.16	19.80

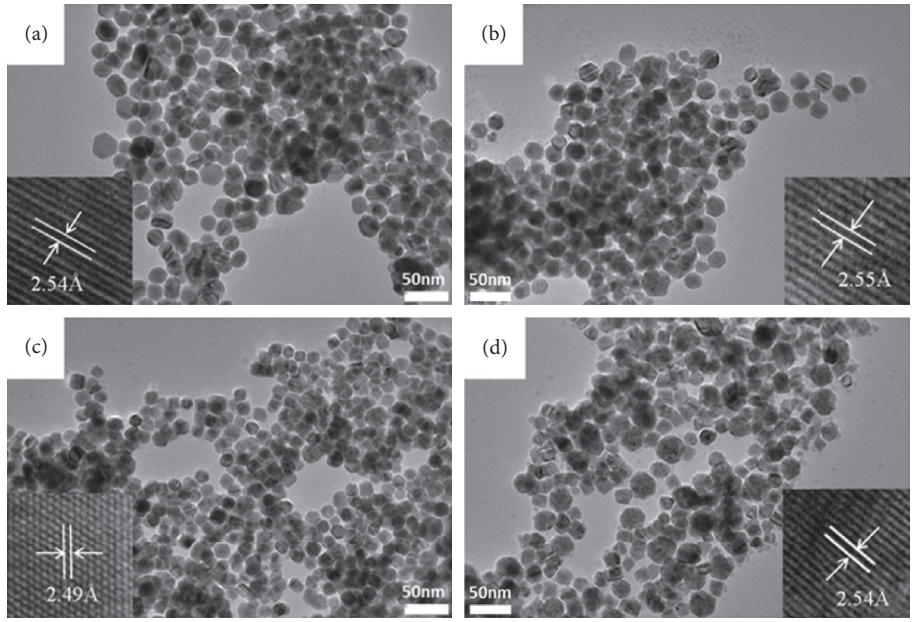

Figure 3: TEM and HRTEM images of PdAg-acac-1 (a), PdAg-acac-2 (b), PdAg-acac-4 (c), and PdAg-acac-5 (d).

25 ± 5 nm, 20 ± 4 nm, 15 ± 3 nm, and 18 ± 4 nm, respectively. The size of PdAg-acac-4 particles was the smallest, which was consistent with the SEM results. Clearly, pure Pd NPs obtained from the same conditions are rather irregular with a broad size range (Figure S1). As shown in the insets of Figure 3, the crystal lattice spacings were around 2.54 Å, 2.55 Å, 2.49 Å, and 2.54 Å corresponding to the (111) crystal plane of PdAg-acac-1, PdAg-acac-2, PdAg-acac-4, and PdAg-acac-5, respectively. Compared to the pure palladium NPs (Figure S1), the crystal plane spacing of the alloy samples is expanded, which is in agreement with the XRD results. To better understand the element distributions of Pd and Ag in the alloy, Figure 4 shows the HAADF-STEM images of singular PdAg-acac-4 NP. These images denote that elements Pd and Ag were evenly distributed in the sample. Ag atoms seem to be located in the center, leading to more Pd atoms than Ag atoms on the surface of single NP.

Electrochemical measurements were carried out to evaluate the catalytic activity of PdAg bimetallic NPs. Figure 5 shows typical CV curves of the PdAg NP-modified glass carbon electrodes (GCEs) in aqueous solutions containing 0.5 M H_2SO_4, 1 M KOH, and 1 M KOH/1 M C_2H_5OH at the same scan rate of 50 mV/s. It can be observed from Figure 5(a) that the typical peak around −0.23~0.1 V is attributed to hydrogen adsorption/desorption on the surface of catalysts. In addition, the characteristic peak and corresponding integral area of PdAg-acac-1 and PdAg-acac-2 are significantly smaller than those of the other two samples, which indicates that more silver atoms might exist on the surface of palladium that reduce active sites on the surface of the catalysts. And then, the reduction of catalytic sites lowers the amount of hydrogen atoms adsorbed, which is further manifested as a decrease in the integral area of the characteristic peak. Furthermore, the featured peak of samples with a certain negative shift around 0.4 V is ascribed to the reduction of Pd oxide, which reveals the enhanced adsorption capacity of the catalyst to oxygen, compared with pure palladium.

Figure 5(b) shows the CV curves of all the PdAg NPs in aqueous 1 M KOH solution. It is clear that the obvious peak appearing around −0.28 V is the reduction peak of Pd oxide, and PdAg-acac-1 shows the most positive peak potential. Moreover, PdAg-acac-4 showed the most negative shift among the four samples, indicating that PdAg-acac-4 had a more active surface consistent with the sequence of the activity of these PdAg NPs in Figure 5(c).

The electrocatalytic activity of PdAg NPs was evaluated by electrooxidation of ethanol on the PdAg NP-modified GCEs, as shown in Figure 5(c). The catalytic peak current densities of PdAg-acac-1, PdAg-acac-2, PdAg-acac-4, and PdAg-acac-5 were about 782, 1406, 2246, and 1838 mA/mg, respectively. The electrochemical active surface areas (ECSAs) of the four samples can be calculated by the reduction region of Pd oxide based on the formula ECSA = Q/(0.424 × Pdm), where Q stands for the corresponding electrical quantity of the integral of the peak from the reduction of Pd oxide [54]. After calculation, the ECSAs of PdAg-acac-1, PdAg-acac-2, PdAg-acac-4, and PdAg-acac-5 were around 112.4, 259.6, 486.3, and 395.2 cm^2/mg, which were consistent with the order of electrochemical activity. It was clear that PdAg-acac-4 has the highest electrocatalytic activity, which can be closely related to the smallest particle size. On the one hand, the small decrease in the size of PdAg-acac-4 with other samples may not fully explain the drastic increase in the ECSAs. On the other hand, the increase of the Pd content in PdAg-acac-4 indicated more Pd atoms on the surface, as shown in Figure 4. In the meantime, the crystal cell enlarged with the Ag content increased, and the corresponding Pd-Pd bond elongated, leading to the downward shift of the d-band center. This may reduce the adsorption

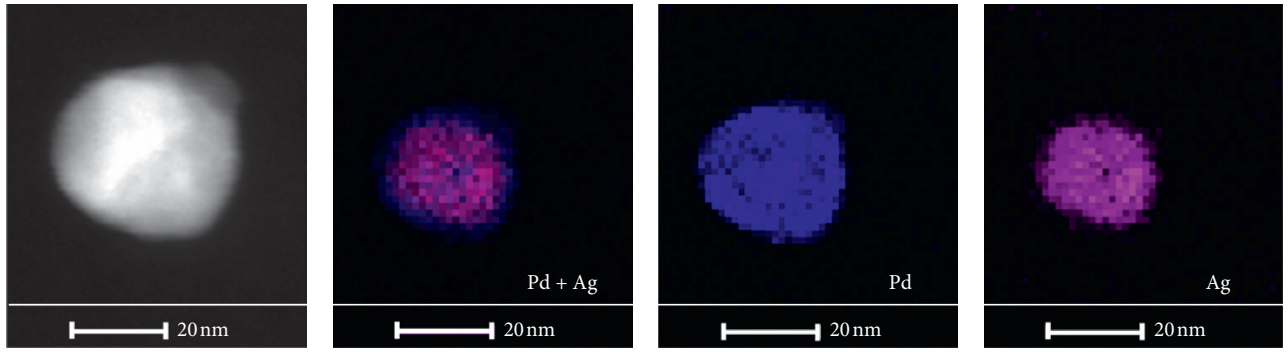

Figure 4: (a) STEM image of PdAg-acac-4 single nanoparticle and EDX element distribution maps of Ag + Pd (b), Pd (c), and Ag (d) in singular nanoparticle.

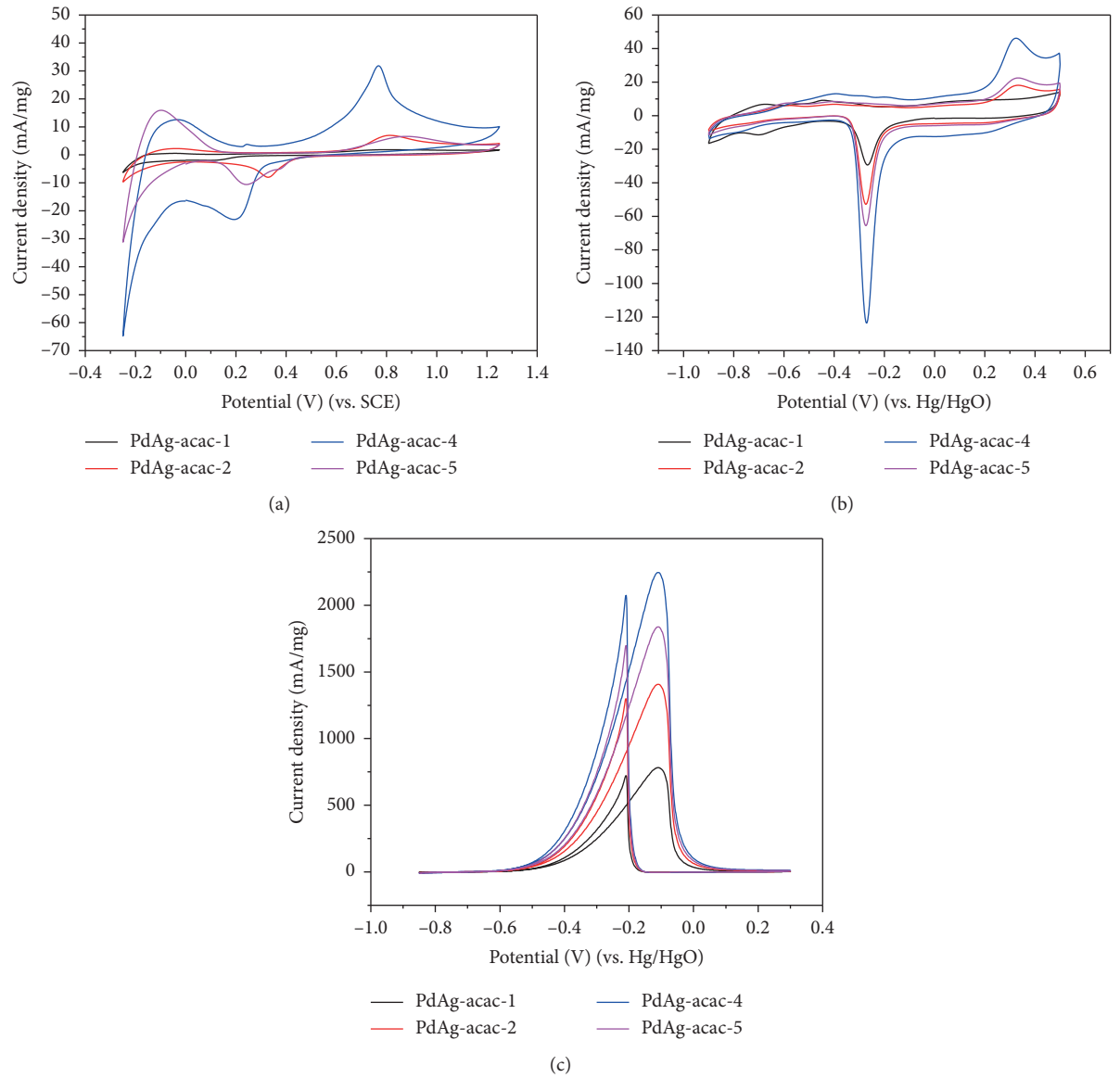

Figure 5: CV curves of the GCEs modified by PdAg-acac-1, PdAg-acac-2, PdAg-acac-4, and PdAg-acac-5 in aqueous solutions containing 0.5 M H_2SO_4 (a), 1 M KOH (b), and 1 M KOH/1 M C_2H_5OH (c) at a scan rate of 50 mV/s.

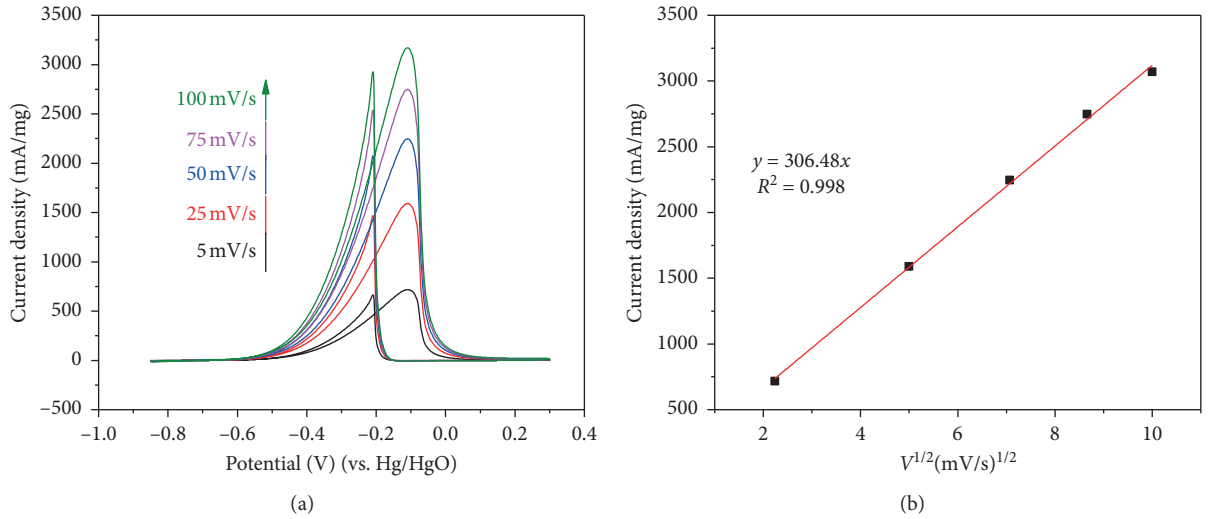

Figure 6: (a) CV curves of PdAg-acac-4 NP-modified GCEs at different scan rates. (b) Corresponding plot of the forward peak current versus the square root of the scan rate.

ability of the alloy NPs to toxic carbon-containing intermediates. Electrochemical data showed that the content of Ag in PdAg NPs has an optimal value for the electrocatalysis of ethanol. Meantime, pure Pd NPs show a catalytic current of about 1263 mA/mg (Figure S2). So, the highest activity of PdAg-acac-4 should be ascribed to the smallest size, the largest ECSA, and synergetic effect between Pd and Ag among all the alloy NPs.

Figure 6(a) shows the CV curves of the PdAg-acac-4-modified GCE for electrooxidation of ethanol at different scanning rates. Obviously, with the scan rate increased continuously, the peak current density of PdAg-acac-4 enhanced accordingly with the peak potential unchanged. As shown in Figure 6(b), it is evident that a linear relationship of the current density with the square root of the scan rate ($V^{1/2}$) is obtained, indicating that the dynamics of the catalytic process of ethanol oxidation occurring on the surface of PdAg-acac-4 NPs is controlled by the diffusion process.

The variations of the peak current density with electrocatalytic cycles of all the PdAg NPs for ethanol oxidation are shown in Figure 7. It is clear that the peak current density of these samples reached the corresponding maximum value within 50 circles of CV measurement, which may be caused by the adsorption of organic residues and the existence of silver atoms on the surface of palladium atoms. This was in accord with those pure NPs with different surface chemistry [55]. And then, the current densities of the four samples were apparently attenuated after 100 cycles. It was obvious that the activity of PdAg-acac-4 was maintained better than any of the others not only after 100 cycles but also after reaching 300 cycles. Although it was faster for PdAg-acac-5 to reach its peak catalytic current density, the cyclic stability was poor, and the activity loss after reaching 300 cycles was large. These phenomena showed that the electrocatalytic performance of the PdAg NPs was increased initially with the gradual increase of the Ag content followed by a decrease in the activity with the Ag content continuously increased.

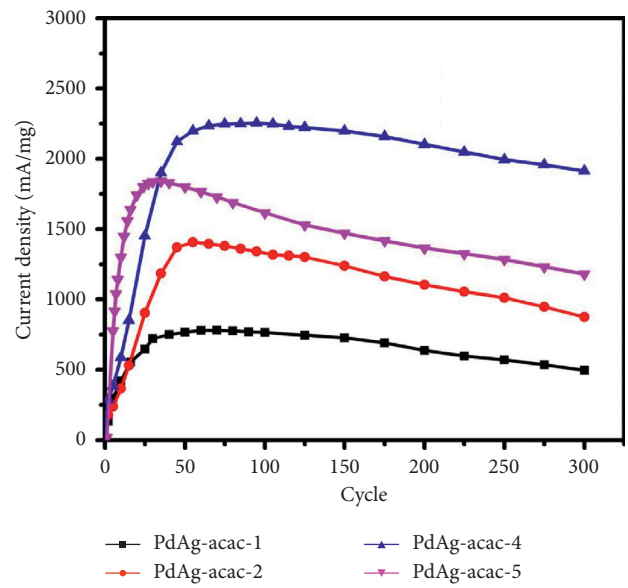

Figure 7: The variation of current density along with the cycle number for ethanol oxidation of the modified GCEs in 1 M KOH/1 M C_2H_5OH solutions at a scan rate of 50 mV/s.

4. Conclusion

A series of well-dispersed PdAg NPs with uniform size and abundant active sites were synthesized via a two-step method. The size of PdAg NPs first decreased with the increase of the Ag content and then increased slightly. However, the lattice constant gradually enlarged with the Ag content within the experimental conditions. Electrochemical measurements showed that the catalytic current density of PdAg-acac-4 with moderate Ag content could reach as high as 2246 mA/mg, the highest among all the alloy PdAg NPs. The enhanced catalytic activity of PdAg-acac-4 can be attributed to both the small size effect and the synergistic effect

in bimetallic electrocatalysis, which will be helpful in the design of bimetallic catalysts with higher performance in the future.

Data Availability

The data used to support the findings of this study are included within the article.

Conflicts of Interest

The authors declare that they have no conflicts of interest.

Authors' Contributions

Fahui Gao and Yanru Yin contributed equally.

Acknowledgments

This work was supported by the National Natural Science Foundation of China (Grant no. 21773133), the World-Class Discipline Program of Shandong Province, and the Taishan Scholar's Advantageous and Distinctive Discipline Program of Shandong Province.

Supplementary Materials

Figure S1: SEM, TEM, and HRTEM images of pure Pd nanoparticles. Figure S2: CV curve of GCEs modified by pure Pd nanoparticles in aqueous solution containing 1 M KOH/1 M C_2H_5OH at a scan rate of 50 mV/s. (*Supplementary Materials*)

References

[1] M. Choun and J. Lee, "Electro-oxidation of mixed reactants of ethanol and formate on Pd/C in alkaline fuel cells," *Journal of Energy Chemistry*, vol. 25, no. 4, pp. 683–690, 2016.

[2] J. Yang, Y. Xie, R. Wang et al., "Synergistic effect of tungsten carbide and palladium on graphene for promoted ethanol electrooxidation," *ACS Applied Materials & Interfaces*, vol. 5, no. 14, pp. 6571–6579, 2013.

[3] E. Hasheminejad, R. Ojani, and J. B. Raoof, "A rapid synthesis of high surface area PdRu nanosponges: composition-dependent electrocatalytic activity for formic acid oxidation," *Journal of Energy Chemistry*, vol. 26, no. 4, pp. 703–711, 2017.

[4] R. Jana, U. Subbarao, and S. C. Peter, "Ultrafast synthesis of flower-like ordered Pd_3Pb nanocrystals with superior electrocatalytic activities towards oxidation of formic acid and ethanol," *Journal of Power Sources*, vol. 301, pp. 160–169, 2016.

[5] J. Yin, L. Zhang, T. Jiao et al., "Highly efficient catalytic performances of nitro compounds and morin via self-assembled MXene-Pd nanocomposites synthesized through self-reduction strategy," *Nanomaterials*, vol. 9, no. 7, p. 1009, 2019.

[6] A. S. Douk, H. Saravani, and M. Noroozifar, "Novel fabrication of PdCu nanostructures decorated on graphene as excellent electrocatalyst toward ethanol oxidation," *International Journal of Hydrogen Energy*, vol. 42, pp. 15149–15159, 2017.

[7] W. Du, K. E. Mackenzie, D. F. Milano, N. A. Deskins, D. Su, and X. Teng, "Palladium-tin alloyed catalysts for the ethanol oxidation reaction in an alkaline medium," *ACS Catalysis*, vol. 2, no. 2, pp. 287–297, 2012.

[8] R. M. Altarawneh and P. G. Pickup, "Pt and PtRu catalyst bilayers increase efficiencies for ethanol oxidation in proton exchange membrane electrolysis and fuel cells," *Journal of Power Sources*, vol. 366, pp. 27–32, 2017.

[9] J. Sánchez-Monreal, P. A. García-Salaberri, and M. Vera, "A genetically optimized kinetic model for ethanol electro-oxidation on Pt-based binary catalysts used in direct ethanol fuel cells," *Journal of Power Sources*, vol. 363, pp. 341–355, 2017.

[10] M. Lv, X. She, Q. Li et al., "Synthesis of magnetic $MnFe_2O_4$/polyaniline composite microspheres and their electrocatalytic activity for oxygen reduction reaction," *Science of Advanced Materials*, vol. 7, no. 9, pp. 1686–1693, 2015.

[11] F. Colmati, G. Tremiliosi-Filho, E. R. Gonzalez, A. Berná, E. Herrero, and J. M. Feliu, "The role of the steps in the cleavage of the C-C bond during ethanol oxidation on platinum electrodes," *Physical Chemistry Chemical Physics*, vol. 11, no. 40, pp. 9114–9123, 2009.

[12] M. Sung and J. Kim, "Oxygen evolution reaction on Pt sphere and Ir-modified Pt sphere electrodes with porous structures," *International Journal of Hydrogen Energy*, vol. 43, no. 4, pp. 2130–2138, 2018.

[13] Y. Shen, B. Gong, K. Xiao, and L. Wang, "In situ assembly of ultrathin PtRh nanowires to graphene nanosheets as highly efficient electrocatalysts for the oxidation of ethanol," *ACS Applied Materials & Interfaces*, vol. 9, no. 4, pp. 3535–3543, 2017.

[14] R. Wang, Q. Liu, T. Jiao et al., "Facile preparation and enhanced catalytic properties of self-assembled Pd nanoparticle-loaded nanocomposite films synthesized via the electrospun approach," *ACS Omega*, vol. 4, no. 5, pp. 8480–8486, 2019.

[15] K. A. Abu-Safieh, A. S. Abu-Surrah, H. D. Tabba et al., "Novel palladium(II) and platinum(II) complexes with a fluoropiperazinyl based ligand exhibiting high cytotoxicity and anticancer activity in vitro," *Journal of Chemistry*, vol. 2016, Article ID 7508724, 7 pages, 2016.

[16] S. Xiong, J. Lan, S. Yin et al., "Enhancing the electrochromic properties of polyaniline via coordinate bond tethering the polyaniline with gold colloids," *Solar Energy Materials and Solar Cells*, vol. 177, pp. 134–141, 2018.

[17] C. Li, M. Iqbal, B. Jiang et al., "Pore-tuning to boost the electrocatalytic activity of polymeric micelle-templated mesoporous Pd nanoparticles," *Chemical Science*, vol. 10, no. 14, pp. 4054–4061, 2019.

[18] C. X. Guo, L. Y. Zhang, J. Miao, J. Zhang, and C. M. Li, "DNA-functionalized graphene to guide growth of highly active Pd nanocrystals as efficient electrocatalyst for direct formic acid fuel cells," *Advanced Energy Materials*, vol. 3, no. 2, pp. 167–171, 2013.

[19] Z. Zhang, L. Xin, K. Sun, and W. Li, "Pd-Ni electrocatalysts for efficient ethanol oxidation reaction in alkaline electrolyte," *International Journal of Hydrogen Energy*, vol. 36, no. 20, pp. 12686–12697, 2011.

[20] Y.-Y. Feng, Z.-H. Liu, W.-Q. Kong, Q.-Y. Yin, and L.-X. Du, "Promotion of palladium catalysis by silver for ethanol electro-oxidation in alkaline electrolyte," *International Journal of Hydrogen Energy*, vol. 39, no. 6, pp. 2497–2504, 2014.

[21] B. Zou, X. S. Chen, J. J. Xia, and C. S. Zhou, "Alkaline ionic liquid modified Pd/C catalyst as an efficient catalyst for oxidation of 5-hydroxymethylfurfural," *Journal of Chemistry*, vol. 2018, Article ID 2018743, 9 pages, 2018.

[22] A.-L. Wang, H. Xu, J.-X. Feng, L.-X. Ding, Y.-X. Tong, and G.-R. Li, "Design of Pd/PANI/Pd sandwich-structured nanotube array catalysts with special shape effects and synergistic effects for

ethanol electrooxidation," *Journal of the American Chemical Society*, vol. 135, no. 29, pp. 10703–10709, 2013.

[23] H. Mao, T. Huang, and A. Yu, "Surface palladium rich Cu_xPd_y/carbon catalysts for methanol and ethanol oxidation in alkaline media," *Electrochimica Acta*, vol. 174, pp. 1–7, 2015.

[24] Y. Wang, Y. Zhao, J. Yin, M. Liu, Q. Dong, and Y. Su, "Synthesis and electrocatalytic alcohol oxidation performance of Pd-Co bimetallic nanoparticles supported on graphene," *International Journal of Hydrogen Energy*, vol. 39, no. 3, pp. 1325–1335, 2014.

[25] J. Zhang, M. Huang, H. Ma, F. Tian, W. Pan, and S. Chen, "High catalytic activity of nanostructured Pd thin films electrochemically deposited on polycrystalline Pt and Au substrates towards electro-oxidation of methanol," *Electrochemistry Communications*, vol. 9, no. 6, pp. 1298–1304, 2007.

[26] H. Huang, Y. Wei, B. Shen et al., "Synthesis of multiple-twinned Pd nanoparticles anchored on graphitic carbon nanosheets for use as highly-active multifunctional electrocatalyst in formic acid and methanol oxidation reactions," *Advanced Materials Interfaces*, vol. 7, no. 11, Article ID 2000142, 2020.

[27] Y. J. Xiong, B. Wiley, J. Y. Chen, Z. Y. Li, Y. D. Yin, and Y. N. Xia, "Corrosion-based synthesis of single-crystal Pd nanoboxes and nanocages and their surface plasmon properties," *Angewandte Chemie*, vol. 117, pp. 8217–8131, 2005.

[28] K. A. Homan, M. Souza, R. Truby et al., "Silver nanoplate contrast agents for in vivo molecular photoacoustic imaging," *ACS Nano*, vol. 6, no. 1, pp. 641–650, 2012.

[29] Y.-F. He, J.-T. Feng, Y.-Y. Du, and D.-Q. Li, "Controllable synthesis and acetylene hydrogenation performance of supported Pd nanowire and cuboctahedron catalysts," *ACS Catalysis*, vol. 2, no. 8, pp. 1703–1710, 2012.

[30] M. S. Ahmed and S. Jeon, "Synthesis and electrocatalytic activity evaluation of nanoflower shaped Ni-Pd on alcohol oxidation reaction," *Journal of The Electrochemical Society*, vol. 161, no. 12, pp. F1300–F1306, 2014.

[31] A.-X. Yin, X.-Q. Min, Y.-W. Zhang, and C.-H. Yan, "Shape-selective synthesis and facet-dependent enhanced electrocatalytic activity and durability of monodisperse sub-10 nm Pt-Pd tetrahedrons and cubes," *Journal of the American Chemical Society*, vol. 133, no. 11, pp. 3816–3819, 2011.

[32] H. Zhao, W. Qi, X. Zhou, H. Wu, and Y. Li, "Composition-controlled synthesis of platinum and palladium nanoalloys as highly active electrocatalysts for methanol oxidation," *Chinese Journal of Catalysis*, vol. 39, no. 2, pp. 342–349, 2018.

[33] M. Yang, X. Lao, J. Sun et al., "Assembly of bimetallic PdAg nanosheets and their enhanced electrocatalytic activity toward ethanol oxidation," *Langmuir*, vol. 36, no. 37, pp. 11094–11101, 2020.

[34] C. Qiu, J. Zhang, and H. Ma, "Fabrication of monometallic (Co, Pd, Pt, Au) and bimetallic (Pt/Au, Au/Pt) thin films with hierarchical architectures as electrocatalysts," *Solid State Sciences*, vol. 12, no. 5, pp. 822–828, 2010.

[35] K. Zhang, D. Bin, B. Yang, C. Wang, F. Ren, and Y. Du, "Ru-assisted synthesis of Pd/Ru nanodendrites with high activity for ethanol electrooxidation," *Nanoscale*, vol. 7, no. 29, pp. 12445–12451, 2015.

[36] X. Yuan, Y. Zhang, M. Cao et al., "$Bi(OH)_3$/PdBi composite nanochains as highly active and durable electrocatalysts for ethanol oxidation," *Nano Letters*, vol. 19, no. 7, pp. 4752–4759, 2019.

[37] G. Sheng, J. Chen, H. Ye et al., "Hollow PdCo alloy nanospheres with mesoporous shells as high-performance catalysts for methanol oxidation," *Journal of Colloid and Interface Science*, vol. 522, pp. 264–271, 2018.

[38] F. Gao, Y. Zhang, F. Ren, Y. Shiraishi, and Y. Du, "Universal surfactant-free strategy for self-standing 3D tremella-like Pd-M (M = Ag, Pb, and Au) nanosheets for superior alcohols electrocatalysis," *Advanced Functional Materials*, vol. 30, no. 16, Article ID 2000255, 2020.

[39] L. Feng, H. Chong, P. Li et al., "Pd-Ni alloy nanoparticles as effective catalysts for miyaura-heck coupling reactions," *The Journal of Physical Chemistry C*, vol. 119, no. 21, pp. 11511–11515, 2015.

[40] M. Wang, W. Zhang, J. Wang et al., "PdNi hollow nanoparticles for improved electrocatalytic oxygen reduction in alkaline environments," *ACS Applied Materials & Interfaces*, vol. 5, no. 23, pp. 12708–12715, 2013.

[41] Y. S. Kang, D. Choi, J. Cho et al., "Highly active and durable ordered intermetallic PdFe electrocatalyst for formic acid electrooxidation reaction," *ACS Applied Energy Materials*, vol. 3, no. 5, pp. 4226–4237, 2020.

[42] W. Wang, R. Wang, S. Ji, H. Feng, H. Wang, and Z. Lei, "Pt overgrowth on carbon supported PdFe seeds in the preparation of core-shell electrocatalysts for the oxygen reduction reaction," *Journal of Power Sources*, vol. 195, no. 11, pp. 3498–3503, 2010.

[43] D. Sengupta, J. Saha, G. De, and B. Basu, "Pd/Cu bimetallic nanoparticles embedded in macroporous ion-exchange resins: an excellent heterogeneous catalyst for the Sonogashira reaction," *Journal of Materials Chemistry A*, vol. 2, no. 11, pp. 3986–3992, 2014.

[44] C. Hu, H. Cheng, Y. Zhao et al., "Newly-designed complex ternary Pt/PdCu nanoboxes anchored on three-dimensional graphene framework for highly efficient ethanol oxidation," *Advanced Materials*, vol. 24, no. 40, pp. 5493–5498, 2012.

[45] K. Jiang, P. Wang, S. Guo et al., "Ordered PdCu-based nanoparticles as bifunctional oxygen-reduction and ethanol-oxidation electrocatalysts," *Angewandte Chemie International Edition*, vol. 55, no. 31, pp. 9030–9035, 2016.

[46] C. Xu, Y. Zhang, L. Wang et al., "Nanotubular mesoporous PdCu bimetallic electrocatalysts toward oxygen reduction reaction," *Chemistry of Materials*, vol. 21, no. 14, pp. 3110–3116, 2009.

[47] J. Xue, G. Han, W. Ye et al., "Structural regulation of $PdCu_2$ nanoparticles and their electrocatalytic performance for ethanol oxidation," *ACS Applied Materials & Interfaces*, vol. 8, no. 50, pp. 34497–34505, 2016.

[48] C. Tang, N. Zhang, Y. Ji et al., "Fully tensile strained Pd_3Pb/Pd tetragonal nanosheets enhance oxygen reduction catalysis," *Nano Letters*, vol. 19, no. 2, pp. 1336–1342, 2019.

[49] N. Ma, S. Wang, X. Liu et al., "PdPb bimetallic nanowires as electrocatalysts for enhanced ethanol electrooxidation," *Science China Materials*, vol. 63, no. 10, pp. 2040–2049, 2020.

[50] F. Gao, Y. Zhang, P. Song et al., "Self-template construction of sub-24 nm Pd Ag hollow nanodendrites as highly efficient electrocatalysts for ethylene glycol oxidation," *Journal of Power Sources*, vol. 418, pp. 186–192, 2019.

[51] X.-J. Liu, X. Yin, Y.-D. Sun et al., "Interlaced Pd-Ag nanowires rich in grain boundary defects for boosting oxygen reduction electrocatalysis," *Nanoscale*, vol. 12, no. 9, pp. 5368–5373, 2020.

[52] C. Peng, Y. Hu, M. Liu, and Y. Zheng, "Hollow raspberry-like PdAg alloy nanospheres: high electrocatalytic activity for ethanol oxidation in alkaline media," *Journal of Power Sources*, vol. 278, pp. 69–75, 2015.

[53] P. Guo, Z. Wei, W. Ye et al., "Preparation and characterization of nanostructured Pd with high electrocatalytic activity,"

Colloids and Surfaces A: Physicochemical and Engineering Aspects, vol. 395, pp. 75–81, 2012.

[54] Y. Gong, X. Liu, Y. Gong et al., "Synthesis of defect-rich palladium-tin alloy nanochain networks for formic acid oxidation," *Journal of Colloid and Interface Science*, vol. 530, pp. 189–195, 2018.

[55] Y. Yin, N. Ma, J. Xue et al., "Insights into the role of poly(vinylpyrrolidone) in the synthesis of palladium nanoparticles and their electrocatalytic properties," *Langmuir*, vol. 35, no. 3, pp. 787–795, 2019.